Laser Beam Polishing of PA12 Parts Manufactured by Powder Bed Fusion

Lukas Eckhardt[1] · Michel Layher[1] · Andreas Hopf[1] · Jens Bliedtner[1] ·
Markus May[2] · Steven Lachmund[2] · Benjamin Buttler[3]

Abstract

Purpose Multi Jet Fusion™ (MJF) is a powder bed fusion technology that fuses material locally with infrared radiation. Fabricated parts show high mechanical strength, low porosity and good dimensional accuracy, even for challenging geometries. They do, however, have a distinctive grainy surface with a roughness of $Ra > 5$ μm limiting possible applications. A fairly recent technology for the smoothing and polishing of polymer surfaces is the surface re-melting by laser beam polishing (LBP). The objective of this study is to characterize the LBP-process of MJF-manufactured Nylon PA12 parts and evaluate it in relation to state-of-the-art finishing methods.

Methods PA12 samples produced using the Multi Jet Fusion™ process are laser beam polished with a 30 W CO_2-laser system. A numerical model is applied in order to estimate the effects of different processing parameters and laser scanning strategies. Calculated temperature progressions are validated experimentally with thermographic measurements. The laser beam polished surfaces are subsequently characterised by surface topography, tensile strength, surface energy and hardness.

Results A re-melting and concurrent smoothing of PA12 surfaces was demonstrated for a number of different processing strategies. The use of a line-focus resulted in the best combination of processing speed, flexibility and surface quality with a reduction in roughness of up to 91%.

Conclusion Laser beam polishing is applicable to parts manufactured by Multi Jet Fusion™. Depending on the case of application, it can be preferable to conventional post-processing strategies for fusing residual powder and improving tribological properties.

Keywords Laser beam polishing · Powder bed fusion · Post-processing · Additive manufacturing

---

Extended author information available on the last page of the article

Introduction

The market for additive manufacturing processes has been expanding strongly for years [1]. An important growth driver is the accelerating adoption of additive manufacturing in series production. This development led to an increasing emphasis on material quality, surface finish as well as production cost and time. One beneficiary of these changes in demand has been the Multi Jet Fusion™ (MJF) technology, introduced by HP in 2016. With already more than 100 million components produced [2], it has proven to be suitable for series production.

MJF uses polymer powder that is fused by infrared radiation. A nozzle array applies a heat-conducting liquid, called fusing agent, and a heat-inhibiting agent, detailing agent, to each layer of powder so that only pre-defined areas fuse. Parts produced this way are mechanically resilient and can reproduce fine details with minimal shape deviations. The most common MJF feedstock is polyamide 12 (PA12). Alternatively, PA11, PP and highly elastic TPU are available [3].

While the technology and the materials used offer enormous potential in terms of component quality, strength and printing speed, application-specific requirements for the surfaces of components often cannot be met. Even after the removal of powder residues, a grainy, rough surface remains, which is susceptible to contamination and may impede subsequent processes. Various post-processing methods have been developed to address this issue and modify surface properties or improve the finish of MJF printed parts.

In general, surface finishing methods for additively manufactured parts can be categorized into processes that apply, remove, or reshape material. The functional principles are either mechanical (sanding, milling, media tumbling, blasting, etc.), chemical (acetone dipping, vapor smoothing, electroless plating, etc.), thermal (laser beam polishing, electrical discharge machining, etc.) or hybrid combinations [4].

The most common post-processing methods for polymer parts manufactured by powder bed fusion include depowdering by bead blasting, coating, dyeing, media tumbling, and vapour smoothing [5, 6]. De-powdering, usually using compressed air containing glass or plastic beads, is a standard post-processing step that is required to clean parts from excess powder. Depending on the blasting media, pressure and time it can already contribute to the smoothing of the surface [7]. A further reduction in roughness is possible by placing parts in a container with abrasive media and vibrating or rotating the container. This process, called media tumbling or barrel finishing, can enhance the surface finish of a component, but it may also remove minor protrusions and round off sharp edges [8, 9]. Another method is vapour smoothing, which involves exposing parts to chemical vapours that solve and reflow the surface layer in order to smoothen even partly enclosed surfaces [10]. Furthermore, protective or decorative layers can be added to the surface by spraying, immersion or electroless plating to modify texture, durability, colour and sheen [11]. All of these techniques can produce a substantial smoothing [8, 10, 11], however they require the use of consumables and may not preserve fine details.

In contrast, laser beam polishing does not require the use of consumables such as abrasive media, chemicals or paint. Instead, a laser beam is directed at the

surface of the part in a controlled manner, melting and resolidifying the surface layer to create a smoother finish. This can be limited locally in order to preserve edges and protruding details. However, laser beam polishing is still a relatively new technique, and the effects of process parameters, including laser power, scanning speed, scanning strategy and trace offset are not fully understood.

The laser beam polishing of parts manufactured by Fused Deposition Modelling has previously been demonstrated successfully [12–15]. While LBP for parts manufactured by powder bed fusion has been mostly limited to metals [16], Braun et al. [17] have shown the feasibility of applying LBP to SLS printed PA12. Optimal results were achieved with in-situ temperature monitoring and processing times of 200 s. However, a viable approach for applying the used scanning strategy to large surfaces has not yet been proposed.

In this article, multiple scanning strategies are evaluated, and their application for Multi Jet Fusion™ parts is tested. The goal is to identify a suitable and scalable strategy in order to reduce the roughness and adapt visual, tactile, and functional properties.

Materials and Methods

Fabrication of Specimens

Parts are fabricated using an HP Jet Fusion 3D 4200 printer with proprietary printing agents and HP 3D High Reusability PA12. Thermal material properties are specified in Table 1. Unless otherwise stated, parts are orientated horizontally in the build chamber and naturally cooled after printing. Specimen dimensions are 50×50 mm² with a thickness of 3 mm for surface characterization and 1 mm for model testing and validation. The maximum polishing angle for 3D-surfaces is determined with concave and convex, cylindrical surfaces having a curvature radius of 20 mm. Powder residue is removed by manually blasting individual parts with glass beads.

Before polishing, specimens are pre-dried at 80 °C for at least 2 h. This is necessary in order to avoid the formation of air blisters due to the evaporation of absorbed water during LBP.

Laser Beam Polishing

Laser beam polishing (LBP) is a post-processing technology using laser radiation in order to locally melt and smoothen surfaces (Fig. 1). When a material-specific process temperature is reached, the resulting roughness is largely determined by the material's melt viscosity and the re-melting time [18].

Depending on the application, this contactless surface treatment can be preferable to conventional finishing technologies as it does not require consumables, avoids material removal or part contamination with abrasives and can be used for a wide variety of polymers [12]. Typical processing speeds range from 0.1 to 2 cm² s^{-1}.
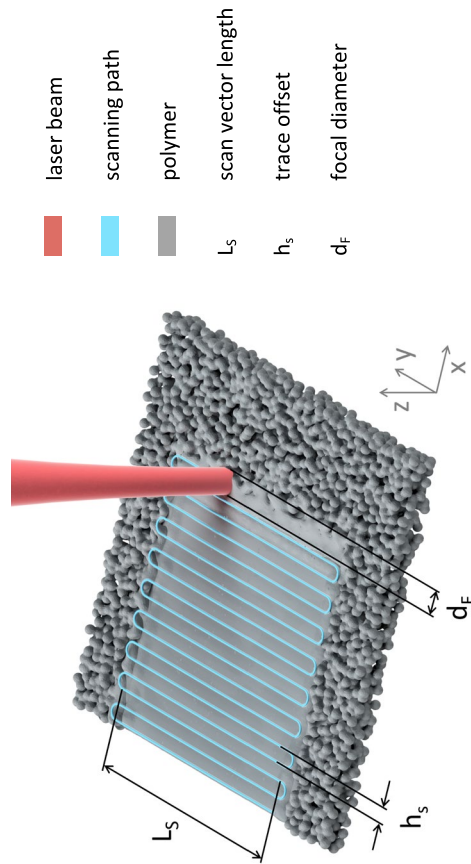
Fig. 1 Illustration of the surface re-melting by laser beam polishing (LBP)

laser beam

scanning path

polymer

L_S scan vector length

h_s trace offset

d_F focal diameter

LBP-experiments are conducted using a Keyence ML-Z9520A 30 W CO_2-laser system and a 3D laser scanning unit with scanning speeds of up to 6 m s^{-1}. Additionally, a fume extraction system is employed during the laser process. The beam profile displays a Gaussian energy distribution with a beam waist, ω_0, of 0.17 mm and a Rayleigh length, z_R, of 6.8 mm. With increasing defocus, z, the half beam diameter, ω, behaves accordingly [19]:

$$\omega(z) = \omega_0 \sqrt{1 + \left(\frac{z}{z_R}\right)^2} \qquad (1)$$

For subsequent calculations a beam with the power, P, is approximated as an ideal Gaussian profile with a corresponding intensity distribution.

$$I(x, y) = \frac{2P}{\pi\omega^2} \exp\left(\frac{-2(x^2 + y^2)}{\omega^2}\right) \qquad (2)$$

A distinction is made between three laser beam polishing strategies which differ in the shape of their respective melt pool. With increasing scanning speed, a meandering beam will produce differently shaped melt pools. Starting from a point-shaped processing zone for quasi-static beams, the thermal energy generated by a faster-moving beam is distributed over a line-shaped and eventually a rectangular area. The latter can be sustained indefinitely by rapidly repeating passes. These strategies are subsequently referred to as point-, line- and areal laser beam polishing. Figure 2 illustrates exemplary scanning paths and resulting thermographic profiles.

The visible increase in temperature is closely related to the input energy density, H [J mm^{-2}]. It can be obtained by integrating the spatially averaged intensity over time. Regarding the introduced scanning strategies, this results in the following relation:

$$H = \frac{mP}{vh_s} \qquad (3)$$

where m, P, v and h$_s$ refer to the total number of passes, the laser power, the scanning speed and the trace offset, respectively.

Model

Interactions between the laser beam and the polymer surface are evaluated using a simple 1D transient heat transfer model. Calculations are implemented in Python and include the surface heating by laser radiation as well as corresponding heat transfers. One necessary input variable is the time dependent beam intensity reaching a given surface increment, dA (Fig. 3). It is determined by substituting the scanning path for the coordinates in Eq. (2). In the model, this calculation is carried out numerically with time increments $\Delta t \leq 200$ μs in order to ensure sufficient accuracy for high scanning speeds as well as the stability of the subsequent numerical solution. An exemplary intensity progression is shown in Fig. 4.
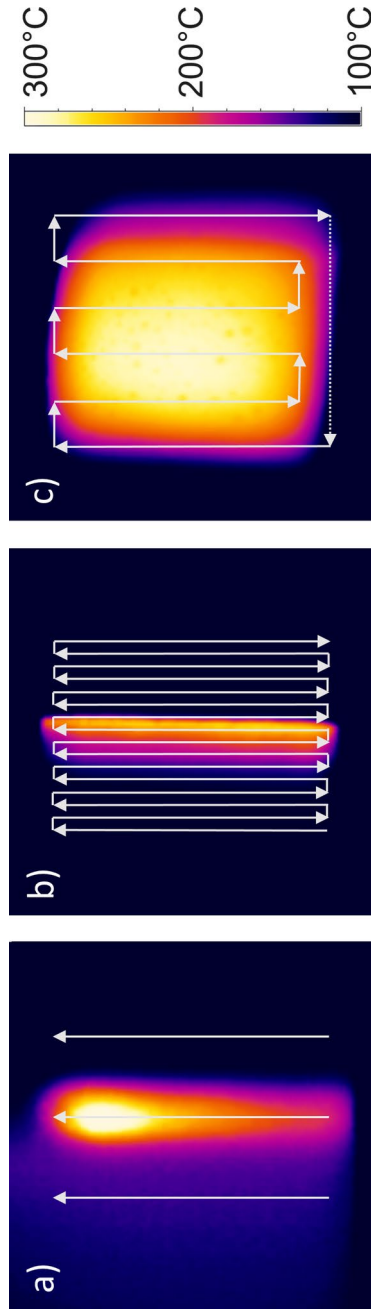
Fig. 2 Investigated scanning strategies: **a** point-LBP where scanning speeds are low and the size of the melt pool is determined by the beam diameter, **b** line-LBP where scanning speeds are high and the size of the melt pool is determined by the scan vector length and **c** areal-LBP where the melt pool is extended to a rectangular area through quickly repeating passes
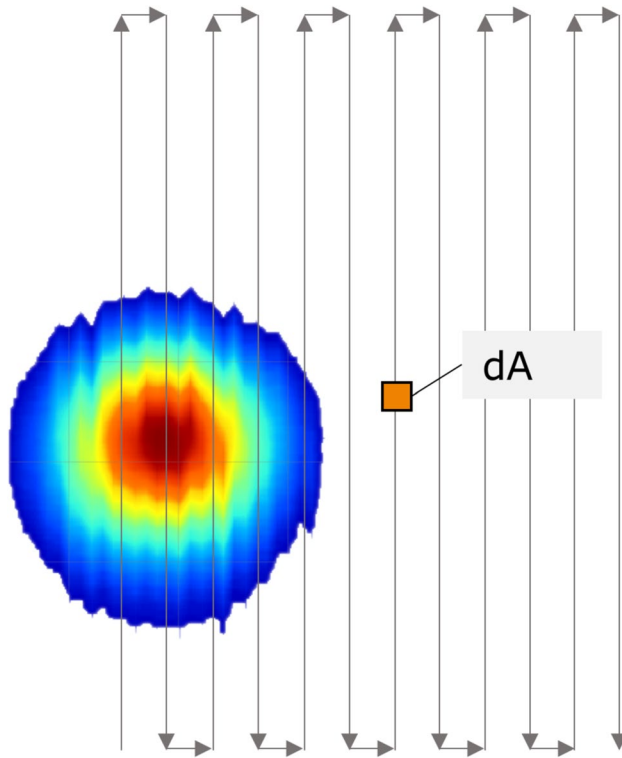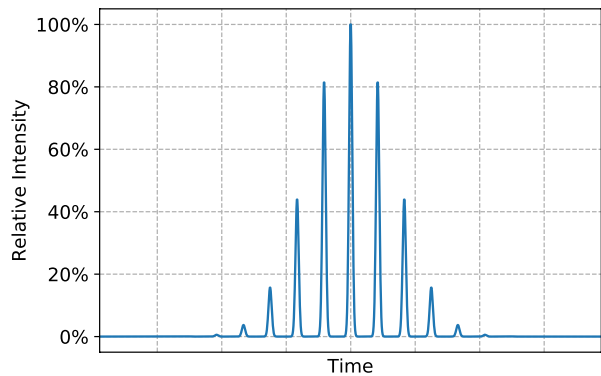
Fig. 3 Exemplary scanning path including the measured beam profile

Fig. 4 Resulting intensity progression for a surface increment dA

Assuming perpendicular beam incidence, the material's refractive index of 1.7 at a wavelength of 10.6 μm [18] causes a reduction of effective intensity by $R = 7\%$ de to reflection. The remaining energy is absorbed and converted to heat in accordance with the Beer-Lambert law. In the model, 50 depth increments with a thickness of

$\Delta z = 20$ µm are considered for calculations. The value of Φ_{abs} corresponds to the absorbed energy per unit of area and time in the respective increment and can be interpreted as the absolute value of heat flux:

$$\Phi_{abs} = (1 - R)I(t)\left(e^{-\alpha z} - e^{-\alpha(z+\Delta z)}\right) \tag{4}$$

Additionally, heat transfer by thermal conduction as well as convection and radiation for external surfaces is considered as follows:

$$\Phi_{exch} = \begin{cases} \frac{\kappa}{\Delta z}\left(T_{n\pm 1} - T_n\right) + \varepsilon\sigma\left(T_{inf}^4 - T_n^4\right) + h\left(T_{inf} - T_n\right), & external \\ \frac{\kappa}{\Delta z}\left(T_{n+1} + T_{n-1} - 2T_n\right), & internal \end{cases} \tag{5}$$

where σ refers to the Stefan-Boltzmann constant and κ, n, ε, T_{inf}, and h are the heat conductivity, layer number, emissivity, ambient temperature and convection coefficient, respectively. The heat flux results in an equivalent change of temperature:

$$_\Delta T = {}_\Delta t \frac{\Phi_{abs} + \Phi_{exch}}{\rho c_p(T)\Delta z} \tag{6}$$

where the initial temperature is set to

$$T(t_0) = 25°C \tag{7}$$

and changes of the specific heat capacity during phase transformations are being approximated with the approach by Peyre et al. [20]:

$$c_p(T) = \begin{cases} c_{p0} + \frac{\Delta H_m}{\sqrt{\pi}(T_{mf} - T_{ms})}\exp\left(-\frac{(T - T_m)^2}{(T_{mf} - T_{ms})^2}\right), & melting \\ c_{p0} + \frac{\Delta H_c}{\sqrt{\pi}(T_{cs} - T_{cf})}\exp\left(-\frac{(T - T_c)^2}{(T_{cs} - T_{cf})^2}\right), & solidification \end{cases} \tag{8}$$

Here c_{p0} is the heat capacity at room temperature and H_m and H_c as well as T_m and T_c denote the melting and crystallization enthalpies and temperatures, respectively. The indices s and f relate to the temperatures at the start and finish of the phase transformation as determined by Defauchy [21]. Whenever no phase changes occur, the specific heat capacity is assumed constant.

The convection coefficient is largely dependent on the air velocity of the fume extraction and was estimated by correlating thermographic measurements with calculation results. Further parameter values are summarized in Table 1. It should be noted, that boundaries between fused powder particles contribute to internal scattering and reduce the penetration depth of laser radiation [18]. When the material starts to melt, internal scattering is reduced. Schuffenhauer et al. [22] observe an increase of CO_2-laser transmission by a factor of approx. 2.5 for 200 µm PA12 layers at melting temperature. This effect largely remains after re-solidification and is considered in the model.

The model omits increased surface absorption due to the initially rough surface, heat conduction in horizontal direction and changes in material properties for

Table 1 Model input parameters

Variable			Value
Attenuation coefficient	α [m^{-1}]	solid	13,000 [18]
		molten/re-solidified	8400
Thermal conductivity	κ [J K^{-1}]		0.3 [18]
Specific heat capacity	c_{p0} [J kg^{-1} K^{-1}]		2670 [18]
Convection coefficient	h [W m^{-2} K^{-1}]		25
Density	ρ [kg m^{-3}]		1010 [23]
Emissivity	ε		0.93
Reflection coefficient	R		0.07
Melting temperature	T_m [K]		460 (187 °C) [23]
Crystallization temperature	T_c [K]		423 (150 °C) [23]
Ambient temperature	T_{Inf} [K]		293 (20 °C)
Melting enthalpy	ΔH_m [J kg^{-1}]		66 [24]
Crystallization enthalpy	ΔH_c [J kg^{-1}]		50 [25]

different cooling speeds and resulting relative crystallizations. Nonetheless it provides useful information for the qualitative comparison of scanning strategies as presented in Section "Scanning Strategies".

Measurement Methods

The thermographic process monitoring is conducted using an Optris Pi 640 infrared camera. It operates at a resolution of 640×118 pixels with 125 frames per second. In order to avoid damaging the micro-bolometer sensor with laser radiation, a previously calibrated lens with a transmission window of 11.5–14 μm is used. Recorded temperatures are averaged over an area of 5×5 pixels.

Unprocessed and polished MJF-parts are characterized by their surface topography, tensile strength, surface energy and hardness. The roughness is measured tactilely with a Taylor Hobson Talysurf i5 in accordance to DIN EN ISO 4287 [26]. Optical measurements using a Polytech TopMap TMS-500 white light interferometer supplement the topography characterization. The ultimate tensile strength is determined with an AMETEK Lloyd LS 5 universal testing machine for five type A-specimen per orientation as described in DIN EN ISO 527-2 [27]. The strength of unprocessed samples is compared to specimens that were polished using line-LBP with a scan vector length of 12 mm and at a laser power of 10 W, a scanning speed of 2 m/s, and a trace offset of 28 μm. A Sauter TI-D durometer test stand measures surface hardness Shore D in accordance with DIN EN ISO 868 [28]. The surface wettability is determined by measuring the contact angle of gently deposited 3 μl water droplets using the dataphysics Contact Angle System OCA 25. A suspected increase in leak-resistance for laser beam polished sealing surfaces is examined by means of a simple positive pressure leakage test as specified in DIN EN 1779 C [29]. For this purpose, the contact surface between two halves of a hollow specimen

is sealed with a rubber gasket and screw-retained with a defined torque. The cavity enclosed is then pressurized via a valve. Potential leaks can be detected by observing the formation of air bubbles while the specimen is immersed in a water basin.

Results and Discussion

Scanning Strategies

PA12-samples with a thickness of 1 mm are used to experimentally verify simulation results for the scanning strategies proposed in Section "Laser Beam Polishing":

– point LBP: quasi-static beam to create a processing zone as large as the beam diameter.
– line LBP: quickly meandering beam to create a quasi-line focus.
– areal LBP: quickly repeating passes to maintain the melt pool over a rectangular area.

Additionally, a distinction is made between fast and slow processing, referring to high power with minimal beam overlap and low power with high beam overlap, respectively. Processing fields have dimensions of 20×20 mm^2 with parameters being based on preliminary polishing experiments. With the exception of areal polishing, where lower temperatures are preferred [17], they are adjusted in order to achieve a maximum surface temperature of roughly 300 °C. Since decomposition does not start until 320 °C, this temperature allows a minimal melt viscosity while achieving optimal polishing results [30].

The stated re-melting time refers to the time during which the material has exceeded the melting temperature and has not yet cooled down below the crystallization temperature. Calculation results for selected processing strategies are illustrated in Fig. 5.

The measured maximum temperatures and re-melting times in Table 2 are in good agreement with the calculation and deviate by an average of 10% and 30%, respectively. The largest temperature differences occur for point polishing as the
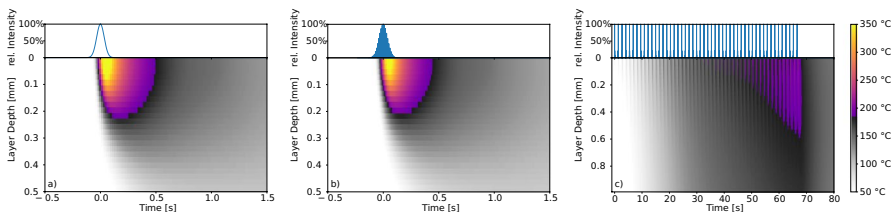

Fig. 5 Simulation results for the scanning strategies **a** point-LBP, **b** slow line-LBP and **c** areal-LBP as described in Table 2. The upper section displays the relative beam intensity over time for a given surface increment. The lower section illustrates resulting temperature changes in the MJF part. Layers highlighted in colour indicate temperatures above the melting point of 187 °C

Table 2 Investigated scanning strategies with numerical and experimental results; Symbols: + suitable, o neutral, - unsuitable result

	laser power P [W]	beam diameter d_F [mm]	trace offset h_s [μm]	scanning speed v [m s^{-1}]	number of passes m	energy density H [mJ mm^{-2}]	processing rate [cm^2 s^{-1}]	simulation		experiment				
								max. temperature [°C]	re-melting time [s]	max. temperature [°C]	re-melting time [s]	thermal deformation	resulting roughness	resulting waviness
point-LBP	2.5	1.5	750	11e-3	1	303	0.1	350	1.0	293	0.5	+	o	-
line-LBP, slow	10	0.34	22	2	1	227	0.4	331	0.9	290	1.1	o	+	+
line-LBP, fast	30	0.34	100	2	1	150	2.0	306	0.6	304	0.6	+	o	o
line-LBP, defocused	10	1.5	14	2	1	349	0.3	282	3.4	279	3.0	o	+	+
areal LBP	10	1.5	220	2	50	1140	0.1	214	43	225	31	-	+	+

growing influence of heat conduction in the horizontal direction with decreasing scanning speed is not considered in the model. Numerical and experimental results allow the following conclusions:

In principle, point-LBP achieves good polishing results as very low scanning speeds facilitate sufficient re-melting times. The processing is heavily localised and only a small fraction of the surface is ever above the melting point. Therefore, thermal distortion is limited and parameters are largely independent of the part geometry. However, the scanning strategy does require stitching of individual paths, resulting in a wavy surface texture.

In pursuit of a better surface quality, line polishing is usually preferred as it can approximate similar intensity progressions without the need for stitching. Resulting temperature profiles are in fact almost identical (Fig. 5a and b) with more of the part's surface being processed simultaneously. A roughness of Ra = 0.6 ± 0.1 μm can be achieved.

With repeating passes, areal-LBP can theoretically enable unlimited re-melting times. It therefore allows the best surface properties with minimal roughness values of Ra = 0.39 ± 0.05 μm. However, long re-melting times and high melting depths are not desirable for dimensional accuracy as thermal deformations become more pronounced. In the case of areal LBP, as shown in Fig. 5c, the 1 mm thick part reaches a temperature of 170 °C throughout. This causes a softening of the material and may result in a concave surface deformation. Furthermore, during areal LBP, the absorbed and emitted amounts of heat per unit of time will eventually compensate for each other, creating a state of thermodynamic equilibrium. This is desirable for long re-melting times but does require a very accurate process control in order to achieve optimal temperatures. In practice, a more sophisticated approach of adjusting laser power in real-time based on temperature measurements as demonstrated by Braun et al. [17] has proven advisable.

In conclusion, each scanning strategy offers individual advantages, depending on the scope of application. Their main difference becomes apparent when considering the scalability for differently sized parts as addressed in Section "Processing Field Scalability".

Processing Field Scalability

In order to polish real-world components, the process must be adaptable to differently sized surfaces. While optimizing for constant field dimensions of 20×20 mm^2, the areal input energy density H [J mm^{-2}] was a useful control variable, as it scales linearly with the focus temperature under constant boundary conditions (Fig. 6).

Once the scan vector length L_S (cf. Fig. 1) is extended however, time intervals between laser passes become longer and more heat is lost to the environment until the beam passes again. As shown in Fig. 7 this leads to decreasing focus temperatures despite constant input energy densities.

There are several ways to compensate for this. Increasing the scanning speed and laser power accordingly is possible to a limited extent. A linear upscaling is however not sufficient as the beam intensity affects the polishing result as well [31].

Fig. 6 Measured focus temperature in relation to energy density for fast line-LBP
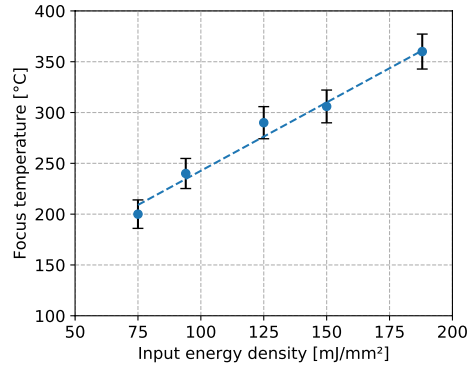
Fig. 7 A decrease in focus temperature becomes evident from thermographic measurements when line polishing with constant input energy density and increasing scan vector length
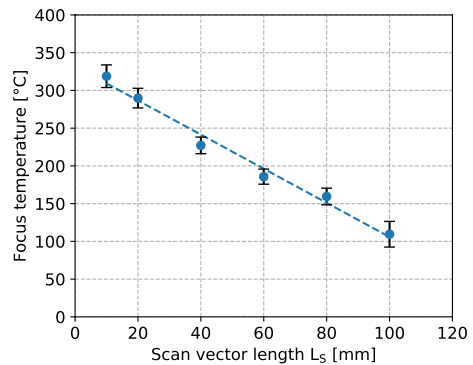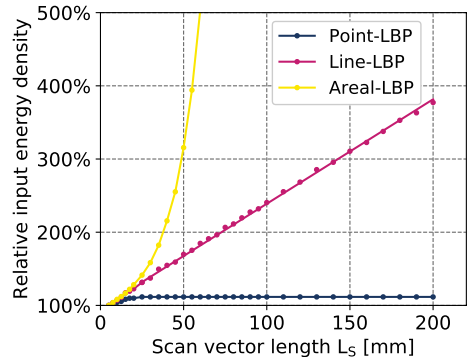
Fig. 8 Simulated relationship between the length of the scan vector and the necessary energy density in order to reach 300 °C surface temperature, normalized for 100% at 5 mm scan vector length

Alternatively, the input energy can be increased by reducing the trace offset. As this strategy is not limited by the systems maximum scanning speed and laser power, the latter approach is subsequently pursued.

In order to adapt to differently sized surfaces, the optimal input energy density for a given scan vector length is calculated using the numerical model. For this purpose, the trace offset h_s is adjusted until a surface temperature of 300 °C is reached. Figure 8 shows the resulting energy densities for the different scanning strategies. It

is evident, that point-LBP is largely independent of processing area, since re-melting only occurs on a locally confined basis. With increasing part size, the necessary energy input converges towards a maximum. For line-LBP the energy density has to be increased linearly with the length of the polishing line (see Section "Process Optimization"). Areal polishing is difficult to scale, as time intervals between passes and the therefore, the necessary energy density increases rapidly. In this case, scaling via scanning speed and laser power would be more appropriate, but the maximum field size is then quickly limited by the system.

In order to achieve both good scalability and high surface quality, the line-LBP scanning strategy is chosen for subsequent experiments.

Process Optimization

In Section "Processing Field Scalability" it has been shown that the energy density necessary to reach 300 °C surface temperature increases linearly with the scan vector length. Equivalent simulations show that this is true regardless of the laser power (Fig. 9, left). Since the flow of the surface layer is however time-dependent as well [18], the polishing result can be affected by the power level used. A low power level requires a low trace offset in order to reach the necessary input energy density (Fig. 9). Consequently, the beam diameter crosses surface increments multiple times and maintains the melt pool. This low-power strategy is ideal to polish small geometries, as high remelting times can be achieved despite rapid successive beam passes. Large parts however, require longer scan vector lengths. Therefore, more time passes between laser interactions resulting in more heat lost to the environment. With low powers of 5–10 W, the necessary surface temperatures of roughly 300 °C can only be achieved with trace offsets of a few micrometres (Fig. 9, right). This results in a very slow and inefficient process. Instead, higher laser powers and consequently higher trace offsets can be used, to process the surface efficiently. Experiments have
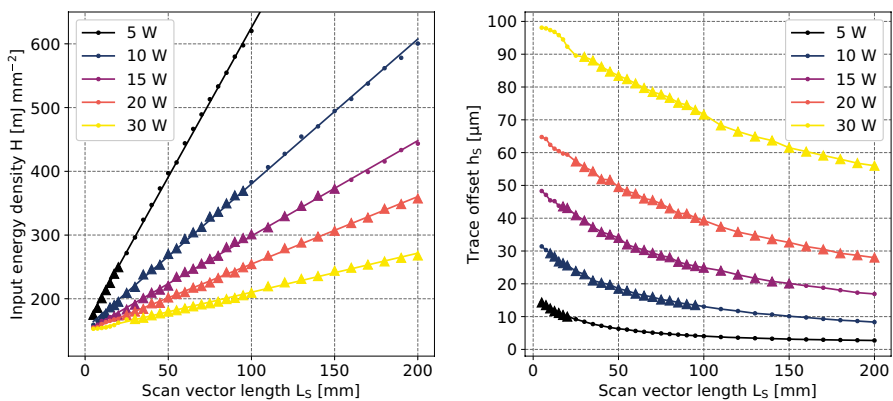

Fig. 9 Line-LBP process window for a scanning speed of 2 m s^{-1} at different laser power levels, each data point represents a set of parameters numerically optimized for a surface temperature of 300 °C with triangle markers indicating well-suited re-melting times of 0.5 to 3 s

shown, that re-melting times of 0.5 to 3 s allow high processing rates, low thermal distortion and a minimal surface roughness. Corresponding sets of parameters are marked with triangles in Fig. 9.

The identified process window is experimentally tested with scan vector lengths of 5, 10, 40, 100 and 200 mm at the given power levels. Additionally, for each sample multiple sets of parameters are examined with higher and lower energy densities than calculated. Resulting surfaces are ranked by roughness. A good agreement between the numerical and experimental results is found and the model is capable of calculating valid parameters. Optimal trace offsets deviate from the calculated value by less than 20% on average, mostly for low trace offsets as the impact of horizontal heat conduction increases.

Finally, studies are extended to non-planar geometries. Commercially available 3D-laser-scanners, like the used Keyence ML-Z9520A system, are able to adjust the focal plane and calculate the scanning speed and trace offset in the planar projection of the 3D surface. The processing of complex part geometries is therefore solely limited by the maximum effective angle of incidence. As this angle increases, the beam profile is distorted and the share of absorbed radiation decreases. Nevertheless, a re-melting and smoothing of the top layer is demonstrated for convex and concave shaped specimens with angles of incidence of up to 80° (Fig. 13e).

Surface Properties

The main purpose of laser beam polishing is a smoothing of the surface. The minimal roughness achieved using line-LBP amounts to Ra = 0.6 ± 0.1 µm or Rq = 0.8 ± 0.1 µm. This is equivalent to an improvement of 91%, compared to the initial surface roughness of Ra = 6.4 ± 0.3 µm or Rq = 8.1 ± 0.4 µm (Fig. 11; Table 3).

These values are similar to the roughness of Sa = 0.61 µm achieved by Braun et al. for an interaction time of 200 s [17], but were realised with a more scalable scanning strategy and an interaction time of only 1.4 s. In comparison, surfaces processed with chemical vapor have a slightly higher surface roughness with minimal values of Ra = 0.78 µm [32] or Sa = 1.4 µm [6].

The measured and numerically calculated depth of the melt pool equals 100–400 µm (Fig. 10), depending on the re-melting time. With an average powder particle size of 60 µm [23], this is sufficient to melt and seal the upper layers of the printed PA12 part. While the visible densification suggests an increase in

Table 3 Surface properties of unprocessed and laser beam polished PA12-surfaces

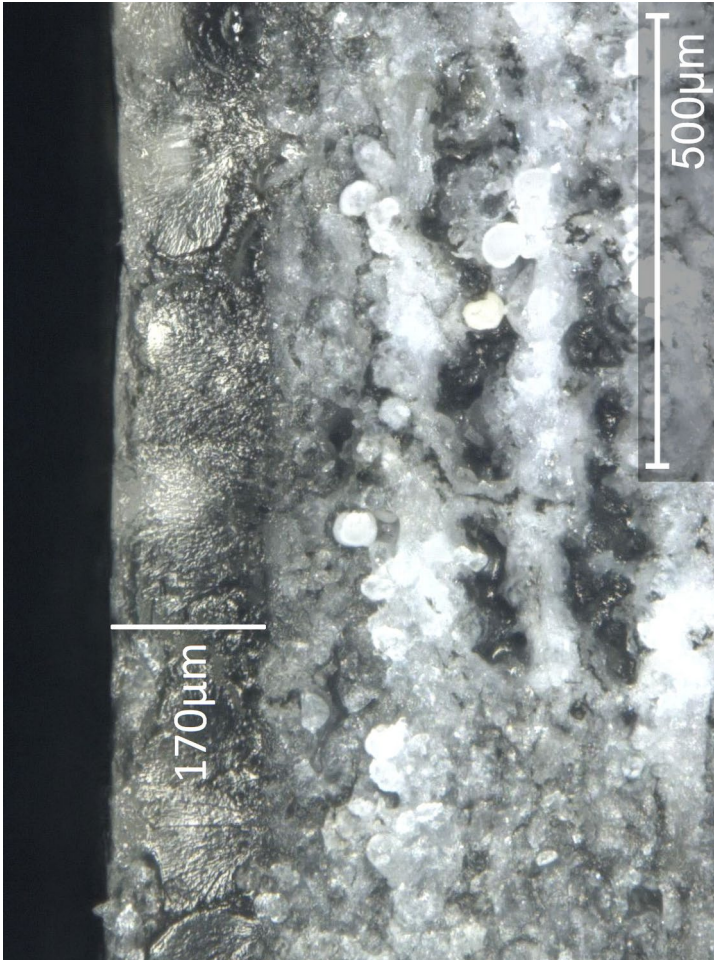|	Unprocessed			Laser beam polished		
Roughness Ra [µm]	6.4 ± 0.3			0.6 ± 0.1		
Roughness Rq [µm]	8.1 ± 0.4			0.8 ± 0.1		
Hardness [Shore D]	73 ± 3			73 ± 3		
Ultimate tensile strength in X, Y and Z [MPa]	41 ± 2,	44 ± 1,	47 ± 1	39 ± 3,	41 ± 3,	45 ± 2
Water droplet contact angle [°]	84 ± 4			59 ± 5		

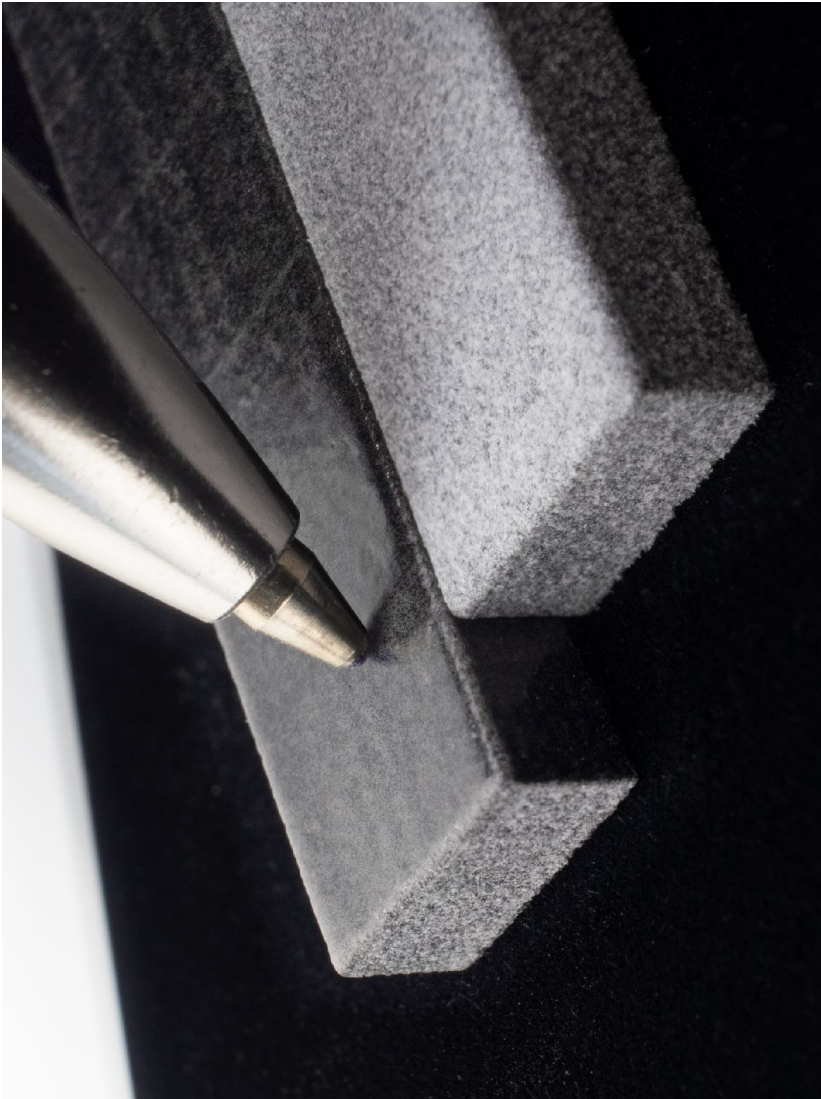**Fig. 10** Cross section of a PA12 part remelted by laser beam polishing

Fig. 11 Resulting surface compared to unprocessed MJF part

surface hardness, this supposed improvement is likely insignificant as the measured hardness remains unchanged at 73 ± 3 Shore D. Furthermore, the mechanical part strength decreases slightly. After LBP, the ultimate tensile strength of rods manufactured in three different build orientations decreases by 6% o average. A likely cause is the introduction of tensile stress in the outer part layers during the cooling phase of LBP (Fig. 11).

The surface wettability is however improved by laser beam polishing. It plays a decisive role for the bonding of coatings and adhesives on polymer parts and can be determined by measuring the contact angle of water droplets [33]. Unprocessed surfaces show a low wettability with an initial contact angle equal to $84° \pm 4°$. This result is related to the formation of air pockets in surface notches and correspondingly an incomplete surface wetting [34]. After polishing the contact angle decreases to $59° \pm 5°$ potentially allowing a more even distribution of adhesives without air pockets and thus better bonding [33, 35].

A remaining challenge is a thermal distortion that can occur for thin-walled PA12-components during laser beam polishing. When the molten, initially stress-free top layer cools on top of the underlying material, it shrinks and therefore deforms the part, comparable to the bimetallic effect [20, 36]. An improvement of the shape retention can be achieved by preheating the components, ideally to the work temperature range (WTR) between T_{cs} and T_{ms} [21] and laser polishing with correspondingly lower energy density. Preliminary tests were limited to preheating temperatures of 80 to 100 °C and showed a 60% decrease in vertical warpage on average. The cooling rate has an additional effect on the deformation, as faster cooling causes greater shrinkage [37]. Optimal LBP results therefore require a temperature-controlled environment. If possible, warpage should additionally be counteracted by an optimised component design e.g. with stiffening ribs or an increased wall thickness.

Applications

Potential applications of the laser polishing process go beyond visually and haptically modified parts. For example, smoothing is advantageous for mechanically strained surfaces. A measure of their load-bearing capacity and wear behaviour is the material ratio, defined in DIN EN ISO 4287 [26]. While the load-bearing material component in the 5 µm sectional plane Rmr(5 µm) for unmachined MJF components is only approximately 1%, aser-beam polished surfaces are already completely dense at this depth (Fig. 12). This indicates an increase in resistance to frictional wear.

At the same time, the fusion of the top layers retains possible powder residues, justifying the use of polished components in dust-sensitive environments. Even medical applications can benefit, as complementary studies suggest that the smoothing and simultaneous closing of surface pores effectively reduces bacterial attachment and growth [32].

MJF fabricated parts have furthermore been found to be suitable for high pressure storage applications, even at elevated temperatures [38]. This results in the need

Fig. 12 Material ratio curve for unpolished and laser beam polished MJF-surfaces
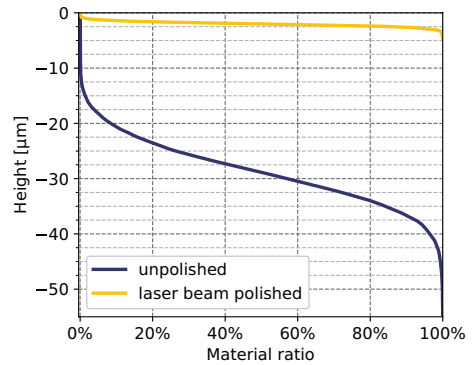
for pressure-tight sealing surfaces. A simple test with a pressurized vessel showed that LBP of the sealing surfaces can help prevent leaking. Compared to the non-processed specimen the maximum pressure of the specific vessel increased by 65% fom 530 to 870 kPa before air started to leak at the detectable rate of 5e-5 mbar l s^{-1}.

In addition, LBP is beneficial as pre-processing for other manufacturing steps. A laser beam texturing of pre-polished surfaces can help to create leather or wood textures as shown in Fig. 13d. This process is easily combined with laser beam marking or localized
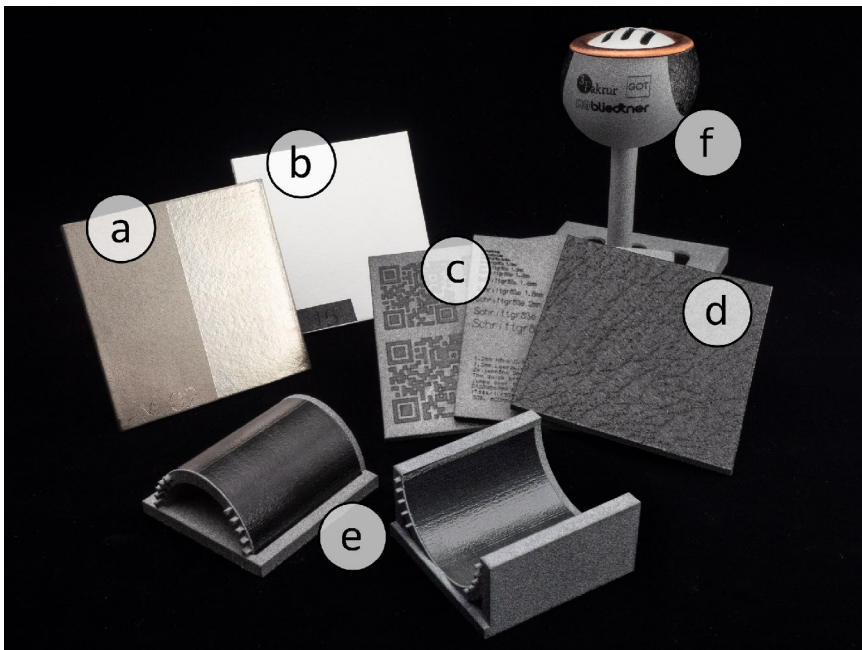
Fig. 13 Specimens with finishing processes: **a** electroless plating, **b** powder coating, **c** laser beam engraving, **d** laser beam texturing, **e** 3D laser beam polishing and **f** a combination of the aforementioned finishing technologies

polishing in order to decorate or label parts (Fig. 13c). The sheen of metallic coatings, applied by electroless plating, is also significantly improved on laser beam polished surfaces, even with a low coating thickness (Fig. 13a, right half). However, powder coating processes do not benefit from LBP, as the surface properties are mostly a result of the powder curing and are independent of the underlying roughness (Fig. 13b).

Conclusions

Laser beam polishing has proven to be a suitable process for the post-processing of MJF components. The derived numerical model can be used to assess different scanning strategies and enables the calculation of suitable processing parameters. Three different scanning strategies have been evaluated. Point-LBP is largely independent of part geometry but does neither achieve high processing speeds nor smooth surfaces. Areal polishing achieves the longest re-melting times and therefore, the best surface quality. However, scaling, especially for large parts, is limited and requires temperature monitoring for optimal results. Line-LBP offers a compromise with good scalability and high surface quality. Due to the invariance to the angle of incidence, this strategy is also applicable to 3D geometries. Polished surfaces are characterized by a high contact area ratio and a low roughness of $Ra = 0.6 \pm 0.1$ µm. However, hardness cannot be measurably improved and tensile strength reduces slightly after LBP.

Potential applications include the improvement of visual, haptical and tribological surface properties as well as the smoothing of sealing surfaces and preparation for further post-processing steps. In combination with laser engraving and conventional coating processes, functional component properties can be modified in various ways.

It is recommendable to investigate the potential of these technologies, including the applicability to other MJF-materials, in further research. Experiments should ideally include a temperature-controlled environment to address the challenge of thermal distortion.

Declarations

Ethical Approval Not applicable.

Competing Interests The authors declare no competing interests.

References

1. Wohlers, T.T., Campbell, I., Diegel, O., Huff, R., Kowen, J.: Wohlers Report 2022: 3D Printing and Additive Manufacturing Global State of the Industry. Wohlers Associates Inc, Fort Collins (2022)
2. Sher, D.: 100 million MJF parts produced to date using HP 3D printers. 3dpbm, 13 09 2021. [Online]. Available: https://www.3dprintingmedia.network/100-million-mjf-parts-produced-to-date-using-hp-3d-printers/. Accessed 17 June 2022
3. HP Development Company, L.P.: HP 3D Printing Materials. (2022). Available: https://www.hp.com/us-en/prianters/3d-printers/materials.html. Accessed 17 June 2022
4. Hashmi, A.W., Mali, H.S., Meena, A.: Improving the surface characteristics of additively manufactured parts: A review. Mater. Today: Proc. (2021)
5. Dizon, J.R.C., Ciara Catherine, H.M.S.C., Gache, L., Cancino, L.T., Advincula, R.C.: Post-processing of 3D-printed polymers. Technologies **9**, 61 (2021)
6. Bazan, A., Turek, P., Zakręcki, A.: Influence of antibacterial coating and mechanical and chemical treatment on the surface properties of PA12 parts manufactured with SLS and MJF techniques in the context of medical applications. Materials **16**, 2405 (2023)
7. O´Connor, H., Dickson, A., Dowling, D.: Evaluation of the mechanical performance of polymer parts fabricated using a production scale multi jet fusion printing process. Addit. Manuf. **22**, 381–387 (2018)
8. Boschetto, A., Bottini, L.: Roughness prediction in coupled operations of fused deposition modeling and barrel finishing. J. Mater. Process. Technol. **219**, 181–192 (2015)
9. Nsengimana, J., Walt, J.V., Pei, E., Miah, M.: Effect of post-processing on the dimensional accuracy of small plastic additive manufactured parts. Rapid Prototyp. J. **25**, 1–12 (2018)
10. Crane, N., Ni, Q., Ellis, A., Hopkinson, N.: Impact of chemical finishing on laser-sintered nylon 12 materials. Addit. Manuf. **13**, 149–155 (2017)
11. 3D Hubs Manufacturing LLC: Post-processing for SLS and MJF 3D printed parts. [Online]. Available: https://www.hubs.com/knowledge-base/post-processing-sls-and-mjf-printed-parts/#how-does-media/bead-blasting-work-for-sls-and-mjf. Accessed 19 04 2023
12. Layher, M., Hopf, A., Eckhardt, L., Bliedtner, J.: Laser beam polishing of polymers. Photonics-Views **16**(3), 83–87 (2019)
13. Chai, Y., Li, R.W., Perriman, D.M., Chen, S., Qin, Q.-H., Smith, P.N.: Laser polishing of thermoplastics fabricated using fused deposition modelling. Int. J. Adv. Manuf. Technol. **96**, 4295–4302 (2018)
14. Chen, L., Zhang, X.: Modification the surface quality and mechanical properties by laser polishing of Al/PLA part manufactured by fused deposition modeling. Appl. Surf. Sci. **492**, 765–775 (2019)
15. Lambiase, F., Genna, S., Leone, C.: Laser finishing of 3D printed parts produced by material extrusion. Opt. Lasers Eng. **124**, 105801 (2020)
16. Gisario, A., Barletta, M., Veniali, F.: Laser polishing: A review of a constantly growing technology in the surface finishing of components made by additive manufacturing. Int. J. Adv. Manuf. Technol. **120**, 1433–1472 (2022)
17. Braun, K., Willenborg, E., Schleifenbaum, H.: Laser polishing as a new post process for 3D-printed polymer parts. Procedia CIRP **94**, 134–138 (2020)
18. Osmanlic, F.: Modeling of Selective Laser Sintering of Viscoelastic Polymers. Dissertation: Friedrich-Alexander-Universität Erlangen-Nürnberg (2019)
19. Bliedtner, J., Müller, H., Barz, A.: Lasermaterialbearbeitung Grundlagen – Verfahren – Anwendungen – Beispiele. Carl Hanser Verlag, München (2013)

20. Peyre, P., Rouchausse, Y., Defauchy, D., Regnier, G.: Experimental and numerical analysis of the selective laser sintering (SLS) of PA12 and PEKK semi-crystalline polymers. J. Mater. Process. Technol. **225**, 326–336 (2015)

21. Defauchy, D.: Simulation du procédé de fabrication directe de pièces thermoplastiques par fusion laser de poudre. Dissertation, Institut des sciences et technologies de Paris (2013)

22. Schuffenhauer, T., Stichel, T., Schmidt, M.: Employment of an extended double-integrating-sphere system to Investigate thermo-optical material properties for powder bed fusion. J. Mater. Eng. Perform. **30**, 5013–5019 (2021)

23. HP Development Company, L.P.: 3D High Reusability PA 12 - Materials Technical Fact Sheet; File 4AA7-1534EEW. 09 2018. [Online]. Available: https://www.spaeh.de/fileadmin/Bilder/Allgemein/pa12-datenblatt.pdf. (Accessed 17 06 2022)

24. Rosso, S., Meneghello, R., Biasetto, L., Grigolato, L., Concheri, G., Savio, G.: In-depth comparison of polyamide 12 parts manufactured by multi jet fusion and selective laser sintering. Addit. Manuf. **36**, 101713 (2020)

25. Plummer, C.J.G., Zanetto, J., Bourban, P.-E., Månson, J.-A.E.: The crystallization kinetics of polyamide-12. Colloid Polym. Sci. **279**, 312–322 (2001)

26. DIN EN: ISO 4287:2010-07 Geometrische Produktspezifikation (GPS) - Oberflächenbeschaffenheit: Tastschnittverfahren - Benennungen, Definitionen und Kenngrößen der Oberflächenbeschaffenheit, Beuth Verlag GmbH

27. DIN EN: ISO 527-2:2012-06 Kunststoffe - Bestimmung der Zugeigenschaften - Teil 2: Prüfbedingungen für Form- und Extrusionsmassen, Beuth Verlag GmbH

28. DIN EN: ISO 868:2003-10 Kunststoffe und Hartgummi - Bestimmung der Eindruckhärte mit Einem Durometer (Shore-Härte), Beuth Verlag GmbH

29. DIN: EN 1779:1999-10 Zerstörungsfreie Prüfung - Dichtheitsprüfung - Kriterien zur Auswahl von Prüfmethoden und -verfahren, Beuth Verlag GmbH

30. Guo, B., Xu, Z., Luo, X., Bai, J.: A detailed evaluation of surface, thermal, and flammable properties of polyamide 12/glass beads composites fabricated by multi jet fusion. Virtual Phys. Prototyp. **16**, S39–S52 (2021)

31. Zhang, W., Wong, K., Morales, M., Molpeceres, C., Arnold, C.B.: Implications of using two low-power continuous-wave lasers for polishing. Int. J. Extreme Manuf. **2**, 035101 (2020)

32. Rybalcenko, K., Folgar, C., Anastasopoulos, I., Ioannides, G., Folgar, L.: Surface processing of additively manufactured articles for the improvement of antimicrobial properties. Trans. Addit. Manuf. Meets Med. **2**(1) (2020)

33. Leicht, H., Orf, L., Hesselbach, J., Vudugula, H., Kraus, E., Baudrit, B., Hochrein, T., Bastian, M.: Adhesive bonding of 3D-printed plastic components. J. Adhes. **96**, 48–63, (2019)

34. Cassie, A.B.D., Baxter, S.: Wettability of porous surfaces. Trans. Faraday Soc. **40**, 546–551, (1944)

35. Bednarek, S., Sokołowski, P., Piwowarczyk, T., Ambroziak, A., Nowak, K., Janowicz, K.: Adhesive bonding of Elements made using the Multi Jet Fusion Additive technique. Biul. Inst. Spawalnictwa. 93–100 (2019)

36. Fahad, M., Hopkinson, N.: Evaluation and comparison of geometrical accuracy of parts produced by sintering-based additive manufacturing processes. Int. J. Adv. Manuf. Technol. **88**, 3389–3394 (2017)

37. Li, J., Yuan, S., Zhu, J., Li, S., Zhang, W.: Numerical model and experimental validation for laser sinterable semi-crystalline polymer: shrinkage and warping. Polymers. **12**, 1373 (2020)

38. Yelamanchi, B., Mummareddy, B., Carradero, C., Santiago, B., Ojoawo, K., Metsger, B., Helfferich, J., Zapka, F., Sillani, E., MacDonald, Cortes, P.: Mechanical and fatigue performance of pressurized vessels fabricated with Multi Jet Fusion™ for automotive applications. Addit. Manuf. **44**, 102048 (2021)

Authors and Affiliations

Lukas Eckhardt[1] · **Michel Layher[1]** · **Andreas Hopf[1]** · **Jens Bliedtner[1]** ·
Markus May[2] · **Steven Lachmund[2]** · **Benjamin Buttler[3]**

✉ Lukas Eckhardt
Lukas.Eckhardt@eah-jena.de

[1] Ernst-Abbe University of Applied Sciences, Carl-Zeiss-Promenade 2, 07745 Jena, Germany

[2] 3Faktur GmbH, Göschwitzer Str. 22, 07745 Jena, Germany

[3] GOT Gesellschaft für Oberflächentechnik mbH, Konrad-Zuse-Straße 4, 07745 Jena, Germany